Hindawi
Shock and Vibration
Volume 2019, Article ID 1612576, 9 pages
https://doi.org/10.1155/2019/1612576

Research Article

Energy Evolution and Acoustic Emission Characteristics of Sandstone Specimens under Unloading Confining Pressure

Tao Qin,[1,2] **Yanwei Duan**,[2] **Hongru Sun**,[2] **Honglei Liu**,[1] **and Lei Wang**[2]

[1]*School of Resources & Civil Engineering, Northeastern University, Shenyang 110819, China*
[2]*Heilongjiang Ground Pressure & Gas Control in Deep Mining Key Lab, Heilongjiang University of Science & Technology, Harbin 150022, China*

Correspondence should be addressed to Tao Qin; 19140270@qq.com

Received 9 July 2019; Revised 16 October 2019; Accepted 28 November 2019; Published 23 December 2019

Academic Editor: Luca Pugi

Copyright © 2019 Tao Qin et al. This is an open access article distributed under the Creative Commons Attribution License, which permits unrestricted use, distribution, and reproduction in any medium, provided the original work is properly cited.

The acoustic emission characteristics of rock specimens under different initial unloading confining pressures were tested to obtain the damage and rupture characteristics of the sandstone unloading confining pressure path. The CT scan and three-dimensional reconstruction of the fractured rock specimens were carried out to study the differences of energy evolution and acoustic emission characteristics during the failure of sandstone under different initial unloading pressures. The results show that the unloading confining pressure has a significant influence on the deformation and failure of the rock. There is a significant yielding platform for the circumferential strain and the bulk strain at the peak of the unloading pressure. The larger the initial unloading pressure is, the greater the axial absorption strain energy, the dissipative energy, and the elastic strain energy are at the peak point. After the stress peak point, the elastic strain can be quickly converted into the dissipative energy for rock damage. The elastic energy released from the moment of rock failure under high confining pressure is more concentrated. The acoustic emission ringing and b value characteristic parameters of the rock have a good correlation with the internal energy evolution of the rock, which better reflects the progressive damage of the rock under low stress and the sudden failure of high-stress unloading.

1. Introduction

During the excavation process of rock underground engineering, the excavation state is in the loading state before excavation. After excavation, the surrounding rock is mostly in the unloading state. That is, the rock mass undergoes the mining dynamics process from the original rock stress, loading, and unloading to destruction. The practice of underground rock engineering shows that most of the rock failures occur in the unloading state of surrounding rock [1, 2]. The study on the failure law of rock damage under unloading confining pressure is of great significance for revealing the mechanical properties and fracture mechanism of rock under the unloading state.

A large number of rock acoustic emission studies have been carried out by scholars at home and abroad to explore the relationship among rock damage, rupture, and acoustic emission characteristics. Acoustic emission of uniaxial and triaxial rocks: The literature [3–10] analyzed the relationship between acoustic emission parameters and rock failure process under uniaxial and triaxial compression of coal and rock and analyzed the acoustic emission characteristics of rock damage and fracture. In terms of unloading confining pressure and cyclic loading and unloading acoustic emission test: Weizhong et al. [11], through the analysis of acoustic emission characteristics of granite under unloading confinement, discussed the characteristics of acoustic emission characteristics of rock failure; Liming et al. [12, 13] carried out the acoustic emission test of marbles under loading and unloading and analyzed the relationship among rock damage, rupture, and acoustic emission characteristics under the loading and unloading path; through the cyclic loading and unloading of coal specimens acoustic emission test, Jun et al. [14] drew a conclusion that cyclic loading and unloading acoustic emission memory effect has advanced characteristics. Mansurov [15] predicted the type of damage based on the acoustic emission phenomenon of the rock mass failure process; Manthei [16] studied the three-axis

acoustic emission characteristics of the rock specimen by using an acoustic emission probe within a resonant frequency range of 20–1000 kHz and drew a conclusion that most of the launch events are caused by tensile cracks made by rock dilatancy.

Acoustic emission characteristic parameters characterizing rock damage and the rupture evolution law have been recognized by more and more scholars. However, acoustic emission as an indirect characteristic parameter is difficult to truly reflect rock internal damage evolution. It is known from the laws of thermodynamics that energy is conserved, and energy transformation is the essence of the process of material change. Damage failure is the state instability phenomenon driven by energy. The deformation failure process of materials always exchanges material and energy with the outside world, and energy conversion reflects the constant changes of material properties. Therefore, damage failure of rock materials can be studied based on the viewpoint of energy balance.

Based on this, the author studies the mechanical properties, energy evolution, and acoustic emission characteristics of sandstone specimens under different initial unloading pressures to explore the characteristics of rock damage, combined with CT scanning and 3D image reconstruction techniques. The failure mechanism and macroscopic failure morphology are analyzed to provide theoretical support for further understanding the fracture mechanism of rock materials.

2. Experimental Plan

2.1. Sandstone Specimens. The rock specimens were taken from Dongrong No. 2 Mine of Heilongjiang Longmei Mining Holding Group and processed cylindrical specimens with a diameter of 50 mm and a height of 100 mm in accordance with the requirements of international rock mechanics tests. The Sonic Viewer-SX ultrasonic speed test system was used to test the acoustic wave of the test piece, and the piece with a similar wave velocity was selected for testing to reduce the discreteness of the test piece.

2.2. Experimental Device. The loading device is a TOP INDUSTRIE Rock 600-50 fully automatic servo rheometer (Figure 1). Two linear variable differential transformers (LVDT) are used to acquire the axial strain, and a circumferential electronic strain gauge is used to collect the circumferential strain. The SH-II type acoustic emission system is used to monitor the acoustic emission characteristics of the rock synchronously.

2.3. Experimental Approach. The loading experiment process is divided into four stages. (1) Initially, loading to the hydrostatic pressure $\sigma_1 = \sigma_2 = \sigma_3$ at a rate of 0.05 MPa/s. (2) Then, the axial pressure was applied at a rate of 0.05 MPa/s to about 80% of the ultimate stress under its confining pressure condition. The ultimate stress was determined by the conventional triaxial compression experiment as shown in Table 1. (3) The stress σ_1–σ_3 was constant, and the confining pressure was unloaded at a speed of 0.05 MPa/s until the rock was destroyed. (4) After the failure, the axial compression was pressed at a rate of 0.1 mm/min until the specimen was completely destroyed. The initial values of unloading confining pressure were taken, respectively, at 5, 10, 15, and 20 MPa. Three rock specimens were tested under each group condition, numbered X5-1, X5-2, X5-3, X10-1, X10-2, X10-3, X15-1, X15-2, X15-3, X20-1, X20-2, and X20-3.

Figure 1: The rock servo-controlled rheology testing machine.

Table 1: Experiment results of rock specimens under different confining pressures.

Serial number	σ_1–σ_3 (MPa)	σ_3 (MPa)
S5-1	121.6	5
S10-1	145.6	10
S15-1	178.5	15
S20-1	194.6	20

During the experiment, the acoustic emission system is used to synchronize the acoustic emission information of the rock. The acoustic emission acquisition system is in sync with the loading system. The SH-II type acoustic emission system is used to monitor the acoustic emission characteristics of the rock. Two acoustic emission sensor probes are arranged on the upper and lower loading ends of the outside of three-axis chamber, and two acoustic emission sensor probes are arranged outside the three-axis chamber wall. The acoustic emission sampling frequency is 2.5 MHz with a gain of 40 dB and a threshold of 30 dB.

3. Deformation and Strength Characteristics of Sandstone under Unloading Confining Pressure

X5-1, X10-3, X15-3, and X20-3 specimens close to the average strength were selected for analysis.

Curves of (σ_1–σ_3)-time, σ_1-time, and σ_3-time of the specimen are shown in Figure 2 ($\sigma_3 = 15$ MPa). The full stress-strain curve of the rock under different initial confining pressures is shown in Figure 3. When the rock is unloaded and the peak strength is reached, the confining pressure decreases, causing the lateral slip of the rock to

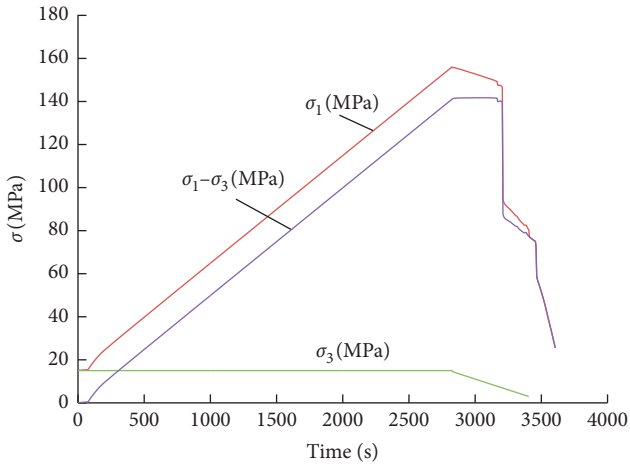

Figure 2: Curves of (σ_1–σ_3)-time, σ_1-time, and σ_3-time of the specimen ($\sigma_3 = 15$ MPa).

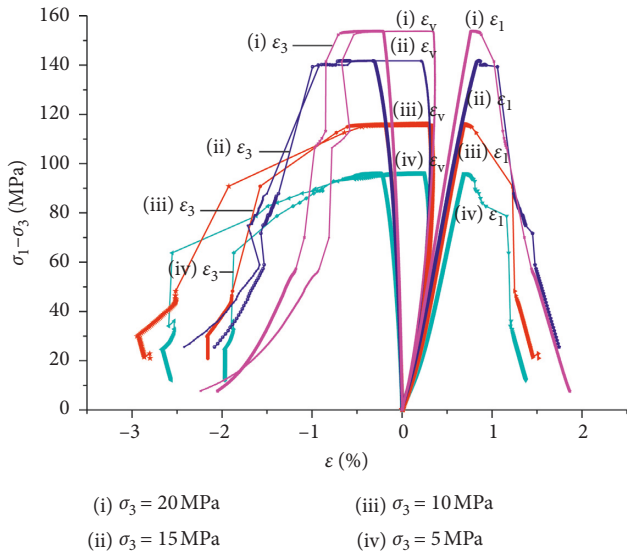

Figure 3: Stress-strain curves of rock specimens under unloading confining pressure.

increase laterally, resulting in an increase in circumferential plastic deformation and a significant deformation yielding platform for the circumferential strain and the bulk strain. Under the unloading pressure, the rock breaks out with a crisp cracking sound. After the damage, the bearing capacity is suddenly lost, and the residual strength is small. This is consistent with unchanged σ_1 and decreased σ_3 in the tunnel wall of the rock underground excavation. The rock unloading is prone to sudden destruction, inducing rock burst.

4. Analysis of Energy Evolution Characteristics

The rock specimen is deformed by external force, and the total input energy generated by the external force on the specimen is U, which is obtained according to the first law of thermodynamics [17]:

$$U = U^{\mathrm{d}} + U^{\mathrm{e}}, \tag{1}$$

where U^{d} is the dissipative energy and U^{e} is the releasable elastic strain energy.

The U^{e} expression is

$$U^{\mathrm{e}} = \frac{1}{2E^t}\left[\sigma_1^2 + 2\sigma_3^2 - 2\nu^t\left(2\sigma_1\sigma_3 + \sigma_3^2\right)\right], \tag{2}$$

where σ_1 and σ_3 are the main stress and E^t and ν^t are, respectively, the unloading elastic modulus and Poisson's ratio at time t.

Triaxial compression test: in hydrostatic stress loading process, testing machine does positive work on the rock specimen, and axial stress σ_1 after hydrostatic stress does positive work on compressive deformation of the rock specimen; while in the circumferential direction, due to the expansion deformation, the strain energy is consumed and confining pressure σ_3 does negative work on the rock specimen. The total strain energy U of a rock specimen can be expressed as

$$U = U_1 + U_3 + U_0, \tag{3}$$

where U_1 is the strain energy of σ_1 axial compression absorption, U_3 is the strain energy consumed by σ_3 for negative work, and U_0 is the strain energy absorbed during the hydrostatic stress state.

The strain energy U_0 stored by hydrostatic stress can be directly obtained according to the theoretical formula of elastic mechanics:

$$U_0 = \frac{3(1-2\nu)}{2E}\left(\sigma_3^0\right)^2, \tag{4}$$

where ν and E are, respectively, initial Poisson's ratio and the elastic modulus.

During the test, the strain energy U_1 absorbed in the axial direction at any time t and the strain energy U_3 consumed by the confining pressure are obtained according to the stress-strain curve integral:

$$\left.\begin{aligned} U_1 &= \int_0^{\varepsilon_1^t} \sigma_1 \mathrm{d}\varepsilon_1, \\ U_3 &= 2\int_0^{\varepsilon_3^t} \sigma_3 \mathrm{d}\varepsilon_3, \end{aligned}\right\}, \tag{5}$$

where ε_1^t is the axial strain at time t and ε_3^t is the hoop strain at time t.

The dissipative energy U^{d} can be expressed as

$$U^{\mathrm{d}} = U_1 + U_3 - U^{\mathrm{e}}. \tag{6}$$

According to the strain energy calculation method, the rock energy evolution characteristics under the unloading confining pressure path are obtained, as shown in Figure 4.

It can be seen that before the unloading pressure, the axial strain energy U_1, the strain energy U_3 consumed by negative work of confining pressure, and the releasable elastic strain energy U^{e} increase significantly with the increase of the axial stress, and the dissipative energy U_{d} increases less, and the curve is relatively straight. After the

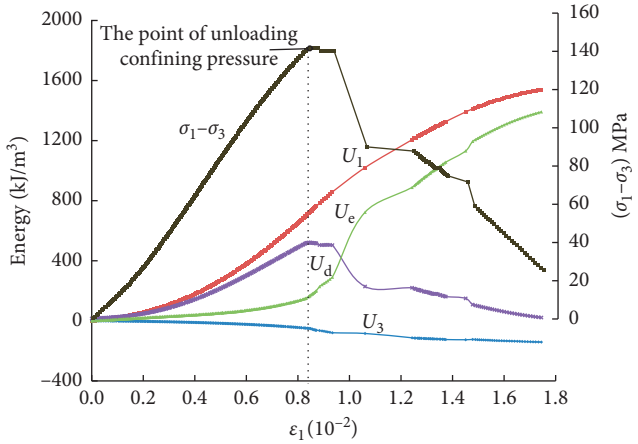

FIGURE 4: Strain energy conversion for the rock specimen ($\sigma_3 = 15$ MPa).

confining pressure releases, although the confining pressure reduces, the circumferential deformation sharply increases, and the strain energy U_3 consumed by negative work of confining pressure obviously increases. However, the internal energy of the rock is mainly the stored releasable elastic strain energy, and the releasable elastic strain energy can be the maximum value at the peak point of the stress. After the stress peak point, the elastic strain can be quickly converted into the dissipative energy used for rock damage failure. The rock under unloading pressure suddenly breaks down, and the rock bearing capacity is small after the failure.

The calculation results of the strain energy at the peak point of the sandstone unloading confining pressure are shown in Table 2. It can be seen from Table 2 that as the confining pressure increases, the peak strength of rock failure increases, and the axial absorption strain energy U_1, the dissipative energy U^d, and the elastic strain energy U^e at the peak point increase significantly with the confining pressure increasing.

5. Analysis of Acoustic Emission and Failure Mode

In this section, the ringing parameters reflecting the frequency of acoustic emission [18] and the b value parameters reflecting the acoustic emission crack size, combined with the energy evolution characteristics of rock failure process, and the acoustic emission features of rock failure process under different initial unloading pressures are analyzed. CT scan was performed on the shape after rock failure, and the three-dimensional shape of the rock specimen failure is reconstructed by using 3D reconstruction and visualization model software.

5.1. Acoustic Emission Counts and Failure Process Analysis. The time-stress-acoustic emission count curve of the rock failure process under different initial unloading pressures is shown in Figure 5. Before the rock specimen is destroyed, the acoustic emission signal is not significantly affected by confining pressure, and the acoustic emission counts are relatively low. With confining pressure unloading, the rock specimen is not affected by confining pressure. When it reaches its bearing limit, the rock specimen suddenly gets damaged. The elastic energy is suddenly released, and the sound emission counts are sharply increased; after the suddenly brittle failure of the rock specimen, the bearing capacity is lost, there is almost no residual strength, and the sound emission counts are suddenly silent.

When the initial values of unloading confining pressure are 5, 10, 15, and 20 MPa, the confining pressures at peak failure are, respectively, 3.32, 4.53, 6.86, and 10.58 MPa. The failure modes are tensile failure, tensile-shear failure, and shear failure. When the initial value of the unloading confining pressure is low, the tensile failure is dominant, and when the initial value of the unloading confining pressure is high, the shear failure is dominant.

During unloading confining pressure, $\sigma_1-\sigma_3$ are kept unchanged, and σ_3 decreases. The analysis of the rock failure mechanism is as follows. In the initial stage of unloading confining pressure, the microcracks in the rock are oriented along the direction of the maximum principal stress under the axial stress. The crack of the rock grows gradually as the confining pressure decreases, and the microcracks are extended along the direction of the maximum principal stress, which causes the tensile crack to expand continuously, which is consistent with the Griffith failure criterion. When the confining pressure is unloaded to a certain extent, the difference rebound deformation caused by unloading causes the tensile stress concentrate on the tip of the crack, and the microfracture tension expands. The tensile crack under the low confining pressure may directly penetrate, and then the tensile fracture mode is formed. In this test, the unloading pressure rate is 0.05 MPa/s. When the initial unloading confining pressure is large, the relatively high confining pressure is maintained during the formation of the main rupture of the rock specimen. The high confining pressure weakens the tensile stress concentration at the crack tip and limits the degree of lateral deformation so that when the initial unloading pressure is high, the releasable elastic energy stored in the rock is large. It can be seen from Table 2 that the larger the confining pressure is, the larger the releasable elastic strain stored at the peak point is. The releasable elastic strain energy of the peak point (peak pressure of 12.95 MPa) is at the initial unloading pressure of 20 MPa, which is 2.42 times of the releasable elastic strain energy of the peak point (peak confining pressure is 4.53 MPa) at the initial unloading pressure of 5 MPa. From the perspective of energy conversion of rocks, the higher the rate of reversible elastic strain energy stored in the rock is, the sudden destruction of the specimen is more severe, and the shear failure of the rock specimen occurs under high confining pressure and high elastic strain energy.

5.2. Analysis of Cumulative Number of Acoustic Emission. The cumulative number of acoustic emission reflects the cumulative damage changes during rock failure. The test results of the cumulative number of acoustic emission of rock specimens under different initial unloading pressures

Table 2: Strain energy at peak strength points or the rock specimen under unloading confining pressure.

Initial value σ_3 (MPa)	Peak value σ_3 (MPa)	$\sigma_1-\sigma_3$ (MPa)	U_1 (kJ·m^{-3})	U_3 (kJ·m^{-3})	U^e (kJ·m^{-3})	U^d (kJ·m^{-3})
5	3.32	96.82	375.50	−46.80	262.82	69.13
10	4.53	117.22	590.30	−118.46	363.89	123.48
15	6.86	141.33	848.59	−183.33	517.71	171.20
20	10.58	156.21	1003.50	−225.64	636.65	176.46

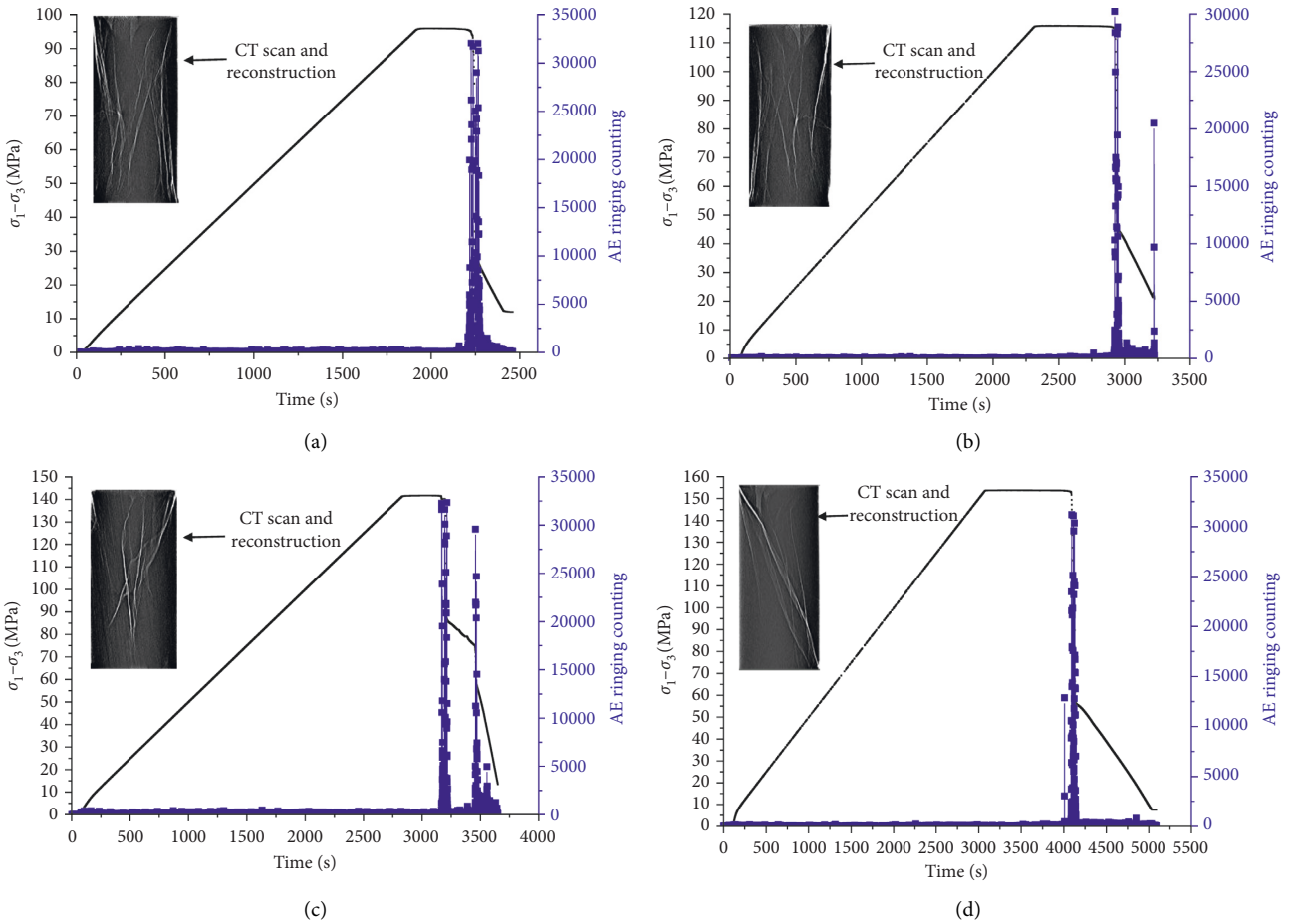

Figure 5: Test results of AE ringing counts of rock specimens under unloading confining pressure. (a) The initial value $\sigma_3 = 5$ MPa. (b) The initial value $\sigma_3 = 10$ MPa. (c) The initial value $\sigma_3 = 15$ MPa. (d) The initial value $\sigma_3 = 20$ MPa.

are shown in Figure 6. Before the rock specimen is destroyed, the curve of the cumulative number of acoustic emission is more stable due to confining pressure, and the cumulative number of acoustic emission is relatively low. With the unloading of confining pressure, the influence of confining pressure gradually weakens on the rock specimen. When the rock specimen reaches its bearing limit, sudden destruction occurs, a large amount of elastic energy is suddenly released, and the cumulative number of acoustic emission increases sharply.

5.3. The Characteristics of Acoustic Emission b Value. The b value is originated from earthquake research. In 1941, Gutenberg and Richter proposed the relationship between earthquake magnitude and frequency, i.e., G-R relation, in the study of seismic activity [18–23]:

$$\lg N = a - bM, \tag{7}$$

where N is the earthquake frequency in the range of ΔM; M is the earthquake magnitude; and a, b is a constant.

The b value is a function of the crack development scale in rock acoustic emission, and the dynamic change of b value has direct physical meaning [12]. The magnitude M is generally replaced by the amplitude of acoustic emission [19–23].

In this paper, the least square method is used to calculate the b value. The sampling window contains 1,000 data of acoustic emission amplitude at a time. The slide window takes 500 data of acoustic emission amplitude. The magnitude interval ΔM is 0.2 dB. In the process of data processing, the intermediate time of each sampling window is taken as the scale of b value. The curve of rock acoustic

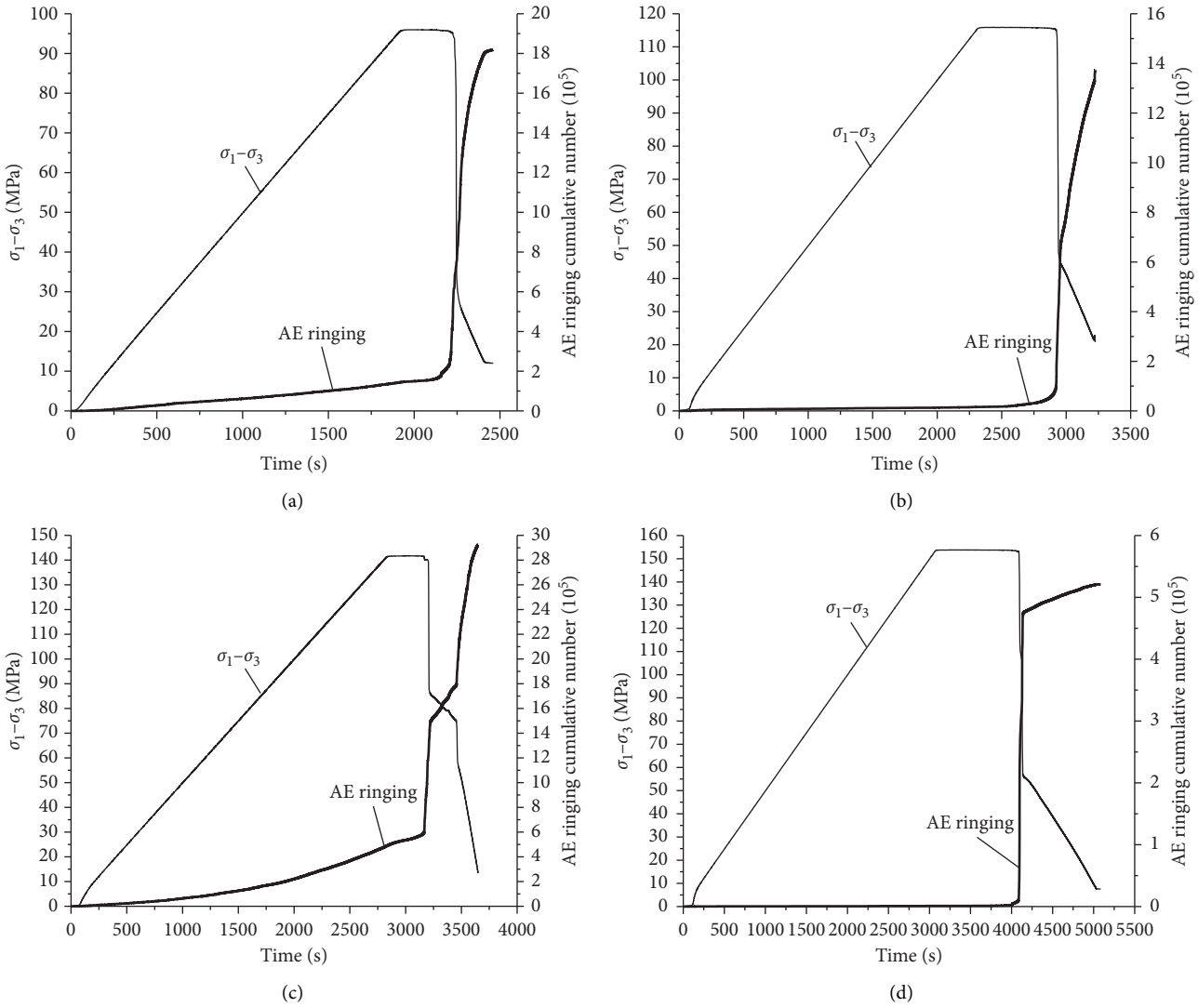

Figure 6: Test results of AE accumulative ringing of rock specimens under unloading confining pressure. (a) The initial value $\sigma_3 = 5$ MPa. (b) The initial value $\sigma_3 = 10$ MPa. (c) The initial value $\sigma_3 = 15$ MPa. (d) The initial value $\sigma_3 = 20$ MPa.

emission b value with time under the unloading confining pressure path is shown in Figure 7.

The b values of rock acoustic emission under different confining pressures are basically the same. Before the peak stress, the small-scale microcracks sprout and expand stably. The energy conversion inside the rock before unloading confining pressure is stable, the dissipative strain energy is fully released, and the b value changes stably before unloading confining pressure. When the peak stress is reached, the microcracks penetrate to form large-scale cracks, and the elastic energy can be quickly converted into dissipative strain energy. The specimen suddenly loses a large amount of energy and generates more acoustic emission events. The b value changes sharply. A large sudden jump in the value indicates a sudden change in the rupture state, representing a sudden instability spread. In the postpeak stage, the b value changes smoothly under low confining pressure, and the b value changes under high confining pressure have a large amplitude change. The main reason is that the microcrack penetrates to become a large crack after the high confining pressure, and the energy that is not fully released in the early part of the loading is released, resulting in more large events, and the b value varies greatly.

6. Discussion

During the excavation in underground projects of deep rock, rock masses have been subjected to the stale of loading-unloading repeatedly before the excavation and the condition of unloading after the excavation. That is, rock masses have been experiencing the mining process from stress of the primary rock, increasing loading and unloading to failure. Safety of the excavation in underground projects is attracting more attention. The study of the damage formation under stress has been a subject of widespread interest, and the results have led to a number of comprehensive texts.

The damage of the rock is a process accompanied by energy input, energy accumulation, energy dissipation,

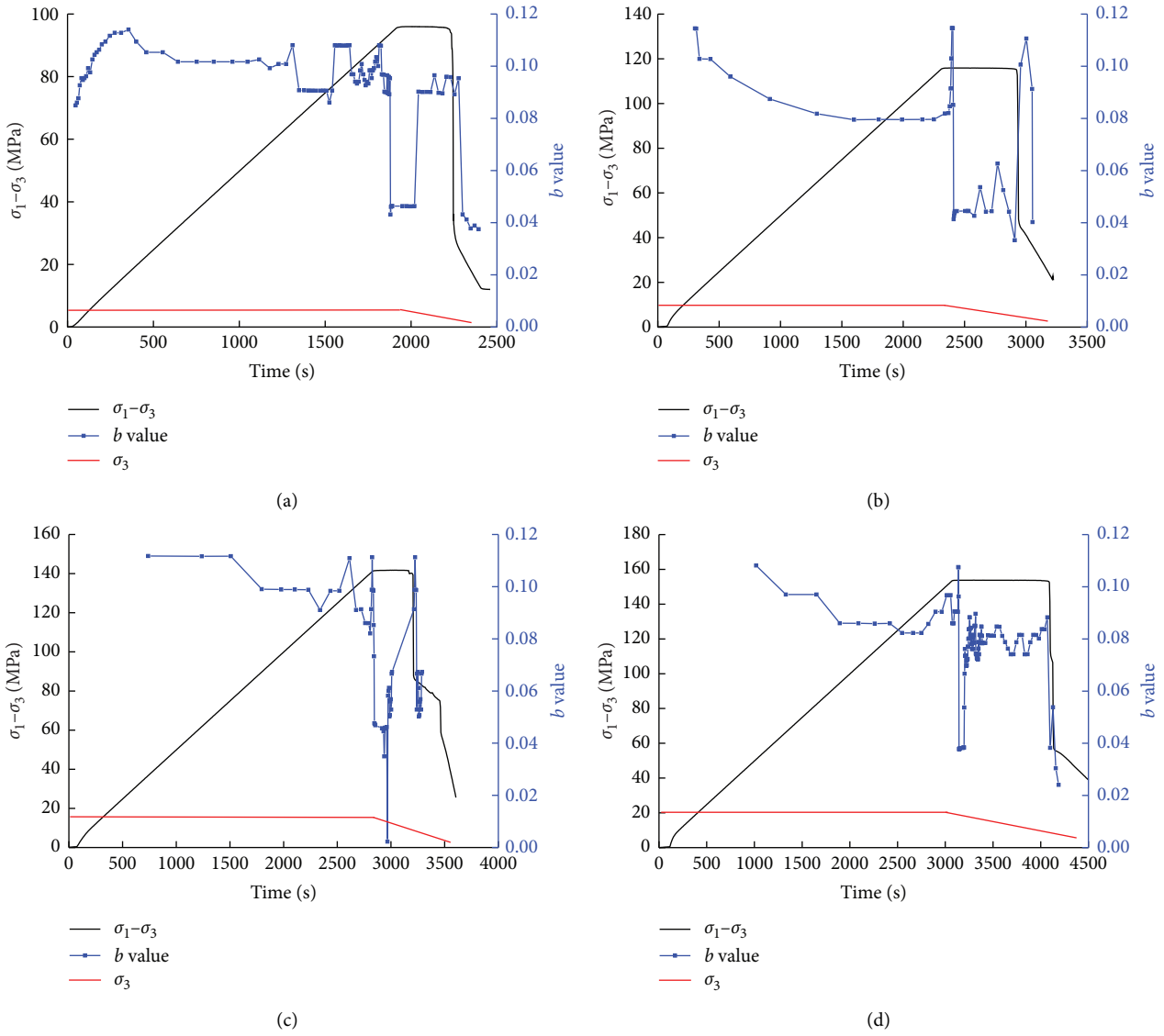

Figure 7: Time-b value of AE curves under unloading confining pressure. (a) The initial value $\sigma_3 = 5$ MPa. (b) The initial value $\sigma_3 = 10$ MPa. (c) The initial value $\sigma_3 = 15$ MPa. (d) The initial value $\sigma_3 = 20$ MPa.

energy release, and energy transformation, as shown in Figure 8. Without considering the thermal energy generated by the change of ambient temperature, part of the external force's work on the rock is accumulated in the form of elastic deformation energy, while the other part is dissipated in the form of plastic deformation energy, damage energy, and so on. When the elastic deformation energy accumulated in the rock reaches the energy storage limit, the rock will be damaged and energy will be released to the outside world, including rock kinetic energy, thermal energy, various radiant energies, and so on. In the process of rock deformation and failure, it is mainly manifested as energy conversion and balance. It is of great significance for understanding and describing the damage evolution of the rock by studying the changes of strain energy, elastic energy, and dissipated energy [24–26]. The study of rock damage process from the perspective of energy, which is closer to the nature of rock

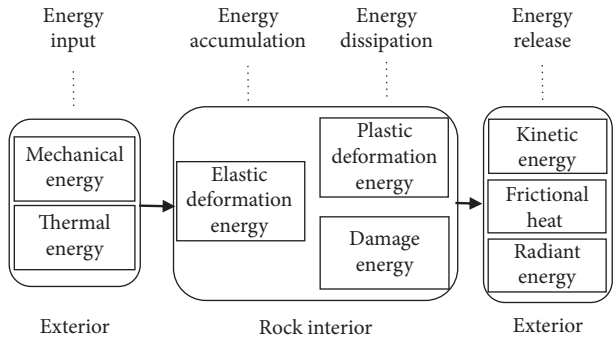

Figure 8: Energy conversion processes of the rock being loaded.

damage, has attracted more and more attention and been applied in engineering practice. Based on the above, the mechanism of rock damage and fracture is discussed based

on energy balance, and some useful conclusions have been drawn in this paper. However, energy evolution is a complex process. In the following research centers, factors such as loading rate, loading path, and size effect should also be considered.

7. Conclusion

In this paper, a series of tests on characteristics of acoustic emission have been performed on sandstone under different initial unloading confining pressures. The CT scan and three-dimensional reconstruction of the fractured rock specimens were carried out to study the differences of energy evolution and acoustic emission characteristics during the failure of sandstone under different initial unloading pressures. The main conclusions are as follows:

(1) Under the unloading pressure path of the rock, the confining pressure decreases and the lateral slip of the rock increases, and the plastic strain platform appears at the peak point at the circumferential strain and the body strain.

(2) The larger the confining pressure is, the axial absorption energy, the dissipative energy, and the elastic strain energy at the peak point are more obviously increased. After the stress peak point, the elastic strain can be quickly converted into the dissipation energy for rock failure. Before unloading confining pressure, the increase of the dissipative energy is small. After unloading the confining pressure, the strain energy for the negative pressure consumption of the confining pressure increases significantly, but the internal energy of the rock is mainly the stored releasable elastic strain energy.

(3) Under the unloading confining pressure path, the rock undergoes strong and sudden brittle failure. The elastic energy released at the moment of rock failure under high confining pressure is more concentrated. And, the sound emission counts are sharply increased.

(4) The rock specimen under the unloading confining path has both tensile and shear failures. The difference rebound deformation caused by unloading causes the tensile stress concentrate on the tip of the crack, and the microfracture tension expands. The tensile crack under the low confining pressure may directly penetrate, and then the tensile fracture mode is formed. The larger the initial unloading pressure is, the greater the releasable elastic energy stored in the rock is. From the perspective of energy conversion of rocks, the higher the rate of reversible elastic strain energy stored in the rock is, the sudden destruction of the specimen is more severe, and the shear failure of the rock specimen occurs under high confining pressure and high elastic strain energy.

(5) The b values of rock acoustic emission under different confining pressures are basically the same. The b value changes smoothly before unloading confining pressure, and the b value changes sharply when the peak stress is reached. The large sudden jump of the b value indicates a sudden change in the rupture state, which represents a sudden instability expansion.

Data Availability

All the data used to support the findings of this study are available from the corresponding author.

Conflicts of Interest

The authors declare that they have no conflicts of interest.

Acknowledgments

This research was supported jointly by the National Natural Science Foundation of China (NNSF) (Grant nos. 51604100, 51774122, and 51674107) and the National Key Research and Development Program (Grant no. 2016YFC0600901).

References

[1] Y. Shuxin, L. Hong, B. Mingzhou et al., "The wall-rock's stress releasing regularity arose by cavern excavation in the high stress condition," *Journal of China Coal Society*, vol. 35, no. 1, pp. 26–30, 2010.

[2] T. Qin, H. Sun, H. Liu et al., "Experimental study on mechanical and acoustic emission characteristics of rock samples under different stress paths," *Shock and Vibration*, vol. 2018, Article ID 4813724, 9 pages, 2018.

[3] W. Enyuan, H. Xueiu, L. Zhentang et al., "Study on frequency spectrum characteristics of acoustic emission in coal or rock deformation and fracture," *Journal of China Coal Society*, vol. 29, no. 3, pp. 289–292, 2004.

[4] X. Jiang, L. Shuchun, T. Xiaojun et al., "Rock fatigue damage evolution based on acoustic emission," *Journal of University of Science and Technology Beijing*, vol. 31, no. 1, pp. 19–24, 2009.

[5] Z. Ru, X. Heping, L. Jianfeng et al., "Experimental study on acoustic emission characteristics of rock failure under uniaxial multilevel loadings," *Chinese Journal of Rock Mechanics and Engineering*, vol. 25, no. 12, pp. 2584–2588, 2006.

[6] L. Shulin, Y. Xiangang, W. Yongjia et al., "Studies on acoustic emission characteristics of uniaxial compressive rock failure," *Chinese Journal of Rock Mechanics and Engineering*, vol. 23, no. 15, pp. 2499–2503, 2004.

[7] J. Hongguang and L. U. Xiang, "Characteristics of acoustic emission and rock fracture precursors of granite under conventional triaxial," *Chinese Journal of Rock Mechanics and Engineering*, vol. 34, no. 4, pp. 694–702, 2015.

[8] J. Hongguang, Z. Yuezheng, J. Yan et al., "Experimental study of confining pressure effect on acoustic emission characteristics of monzonite granite under triaxial compression," *Chinese Journal of Rock Mechanics and Engineering*, vol. 31, no. 6, pp. 1162–1168, 2012.

[9] S. Chengdong, Z. Xinxian, L. Baofu et al., "Experimental study of the characteristics of acoustic emission for sandstone specimens under uniaxial and triaxial compression tests," *Journal of Mining and Safety Engineering*, vol. 28, no. 2, pp. 225–230, 2011.

[10] Z. Xingguang, M. Like, S. Rui et al., "Fracture evolution and strength characteristics of Beishan deep granite ender compression conditions," *Chinese Journal of Rock Mechanics and Engineering*, vol. 33, no. S2, pp. 3665–3675, 2014.

[11] C. Weizhong, L. Senpeng, G. Xiaohong et al., "Unloading confining pressure for brittle rock and mechanism of rock burst," *Chinese Journal of Geotechnical Engineering*, vol. 32, no. 6, pp. 963–969, 2010.

[12] Z. Liming, M. Shaoqiong, R. Mingyuan et al., "Acoustic emission frequency and b value characteristics in rock failure process under various confining pressures," *Chinese Journal of Rock Mechanics and Engineering*, vol. 34, no. 10, pp. 2057–2063, 2015.

[13] Z. Liming, W. Zaiquan, S. Lei et al., "Acoustic emission characteristics of marble during failure process under different stress paths," *Chinese Journal of Rock Mechanics and Engineering*, vol. 31, no. 6, pp. 1230–1236, 2012.

[14] H. Jun, P. Jienan, and W. Anhu, "Acoustic emission characteristics of coal specimen under triaxial cyclic loading and unloading," *Journal of China Coal Society*, vol. 39, no. 1, pp. 84–90, 2014.

[15] V. A. Mansurov, "Acoustic emission from failing rock behaviour," *Rock Mechanics and Rock Engineering*, vol. 27, no. 3, pp. 173–182, 1994.

[16] G. Manthei, "Characterization of acoustic emission sources in a rock salt specimen under triaxial compression," *Bulletin of the Seismological Society of America*, vol. 95, no. 5, pp. 1674–1700, 2005.

[17] X. He-ping, J. Yang, and L. Li-yun, "Criteria for strength and structural failure of rocks based on energy dissipation and energy release principles," *Chinese Journal of Rock Mechanics and Engineering*, vol. 24, no. 17, pp. 3003–3010, 2005.

[18] Q. Tao, S. Hongru, L. Heng, Z. Jun-wen, L. Gang, and J. Yuannan, "Experimental study on mechanical and acoustic emission characteristics of sandstone samples under different confining pressure," *Journal of Heilongjiang University of Science and Technology*, vol. 28, no. 2, pp. 130–135, 2018.

[19] S. Cox and P. G. Meridith, "Micro cracking formation and material softening in rock measured by monitoring acoustic emissions," *International Journal of Rock Mechanics and Mining Sciences*, vol. 30, pp. 11–24, 1983.

[20] D. L. Turcotte, W. I. Newman, and R. Shcherbakov, "Micro and macroscopic models of rock fracture," *Geophysical Journal International*, vol. 152, no. 3, pp. 718–728, 2003.

[21] C. G. Hatton, I. G. Main, and P. G. Meredith, "A comparison of seismic and structural measurements of scaling exponents during tensile subcritical crack growth," *Journal of Structural Geology*, vol. 15, no. 12, pp. 1485–1495, 1993.

[22] M. V. M. S. Rao and K. J. Prasanna Lakshmi, "Analysis of *b*-value and improved *b*-value of acoustic emissions accompanying rock fracture," *Current Science*, vol. 89, pp. 1577–1582, 2005.

[23] F. Bin, Z. Zonghong, W. Haiquan et al., "Precursor information study on acoustic emission characteristics of marble under uniaxial cyclic loading-unloading," *Journal of China Coal Society*, vol. 41, no. 8, pp. 1946–1953, 2016.

[24] X. Heping, P. Ruidong, J. U. Yang et al., "On energy analysis of rock failure," *Chinese Journal of Rock Mechanics and Engineering*, vol. 24, no. 15, pp. 2603–2608, 2005.

[25] Z. Yang, L. Xibing, Z. Zilong et al., "Energy evolution and stress redistribution of high-stress rock mass under excavation disturbance," *Chinese Journal of Geotechnical Engineering*, vol. 34, no. 9, pp. 1677–1684, 2012.

[26] C. Yu, W. Zaiquan, Z. Yingren et al., "Energy evolution principle of fracture propagation of marble with different unloading stress paths," *Journal of Central South University (Science and Technology)*, vol. 47, no. 9, pp. 3140–3147, 2016.

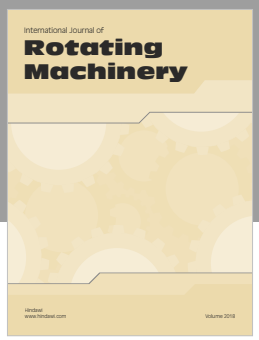

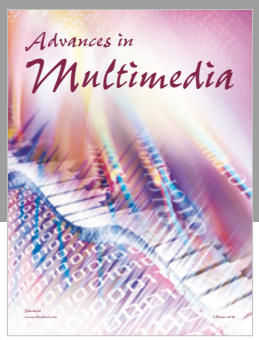

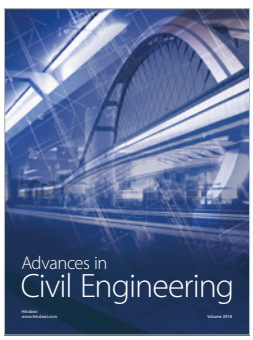

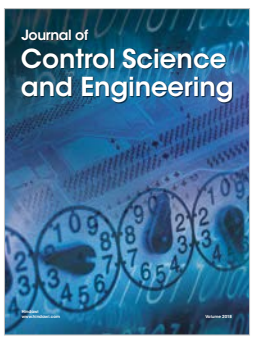

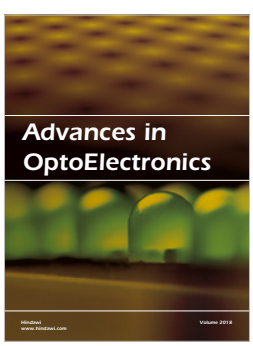

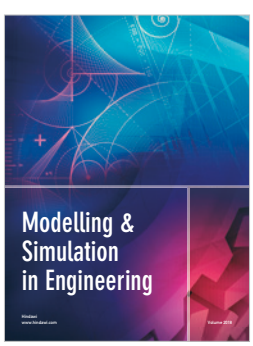

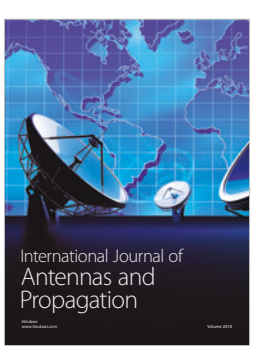

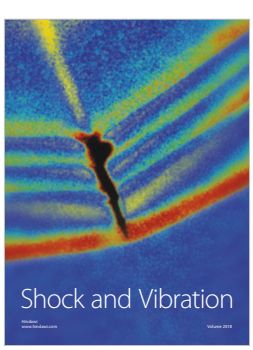

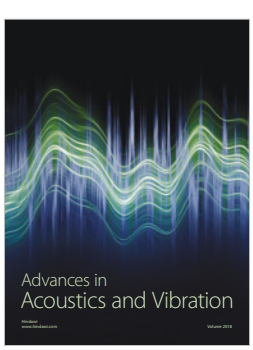

Hindawi

Submit your manuscripts at
www.hindawi.com